PERGAMON

Chemical Engineering Science 54 (1999) 2055–2065

Chemical Engineering Science

An experimental and numerical study of turbulent swirling flow in gas cyclones

A.J. Hoekstra*, J.J. Derksen, H.E.A. Van Den Akker

Kramers Laboratorium voor Fysische Technologie, J.M. Burgers Centre for Fluid Mechanics, Delft University of Technology, Prins Bernhardlaan 6, 2628 BW Delft, Netherlands

Abstract

Experimental results on the turbulent, strongly swirling flow field in a reverse flow gas cyclone separator are presented, and used to evaluate the performance of three turbulence closure models. Mean and fluctuating velocity components were measured for gas cyclones with different geometric swirl numbers by means of laser-Doppler velocimetry. The experimental data show the strong effect of the geometric swirl number on mean flow characteristics, in particular with respect to vortex core size and the magnitude of the maximum tangential velocity. It is shown that the forced vortex region of the flow is dominated by the so-called precessing vortex core. Numerical calculation of the cyclonic flow shows that turbulence models based on the eddy-viscosity approach fail to predict the combined vortex observed experimentally. Predictions with the Reynolds stress transport model are in reasonable agreement with measured profiles for all three swirl numbers, though the turbulent normal stresses are generally overpredicted.

Keywords: Gas cyclone; Swirl flow; Laser-Doppler velocimetry; Computational fluid dynamics; Reynolds stress transport model

1. Introduction

Gas cyclone separators are widely used in the petrochemical and process industries to separate dust from gas streams or for product recovery. Their geometrical simplicity, their relative economy in power, and their flexibility with respect to high temperature and pressure explain their suitability in industrial dedusting. An important application is the recovery of catalyst in fluid catalytic cracking units (FCCU). Here, the gas cyclone is generally used in a multi-cell arrangement to meet recovery requirements of typically $>99\%$. At a further stage, a high-efficiency cyclone system may be used to remove the remaining particles. The gas cyclone used at this stage operates at low solids loading, with the particles having a particle diameter in the range of 0.1–80 μm. High collection efficiencies ($>99.9\%$) are demanded, e.g., to meet environmental regulations on dust emission and/or to prevent excessive wear of turbine blades in energy recovery systems.

The conventional way of predicting the collection performance of gas cyclones is based on (semi-) empirical modelling. Most theories take into account the effects of particle size, particle density, gas velocity and kinematic viscosity, as well as of the effects of dimensions and geometry of the cyclone. The collection efficiency of a cyclone may be described in terms of the cut-size or critical particle diameter, which represents the particle size that corresponds to 50% collection efficiency. Based on the 'static particle' approach, equations for particle collection were developed by Stairmand (1951) and Barth (1956). This approach involves determining the particle diameter for which the centrifugal force on the particle is exactly balanced by the inward drag force. To calculate the cut-size of a specific cyclone geometry, two parameters need to be estimated: the tangential velocity, v_t, of the air flow at the edge of the cyclone core, and the length, h^*, of the cyclone core. These parameters take the geometrical dimensions of the cyclone implicitly into

* Corresponding author. Fax: 31 15 2782838; e-mail: arjen@klft.tn.tudelft.nl.

0009-2509/99/$ – see front matter
PII: S0009-2509(98)00373-X

account. Expressions for these parameters were derived from experimental results by Barth (1956), and more recently by Iozia and Leith (1989). Other cyclone models allow for the calculation of the grade efficiency curve for any specific geometrical lay-out of a cyclone (see, e.g., Leith and Licht (1972) and the three-region model of Dietz (1981)). Also in these models, analytical expressions are used to describe the main gas flow field characteristics, such as the size of the vortex core and the distribution of the tangential velocity component.

The exploitation of computational fluid dynamics (CFD) software for the numerical calculation of the gas flow field is a more generic way of modelling, and may, in principle, yield better predictions on the collection performance of a cyclone. One of the first CFD calculations of the flow in an industrial cyclone was done by Boysan (1982). An important issue that needs to be addressed for this type of calculations is the effect of turbulence on the gas flow field. Turbulent closure models known in literature for Eulerian frameworks have some weaknesses and modelling uncertainties (see, for example, the review on closure models by Hanjalić, 1994), and their performance still needs to be judged by experimental data.

The aim of this study is to evaluate the performance of the k–ε model, the RNG-k–ε model, and the Reynolds stress transport model (RSTM) in predicting the gas flow field in a cyclone separator. Tangential and axial velocity components were measured in the separation zone of the cyclone by means of laser-Doppler velocimetry (LDV). The measurements were done in a model cyclone with a varying exit pipe diameter.

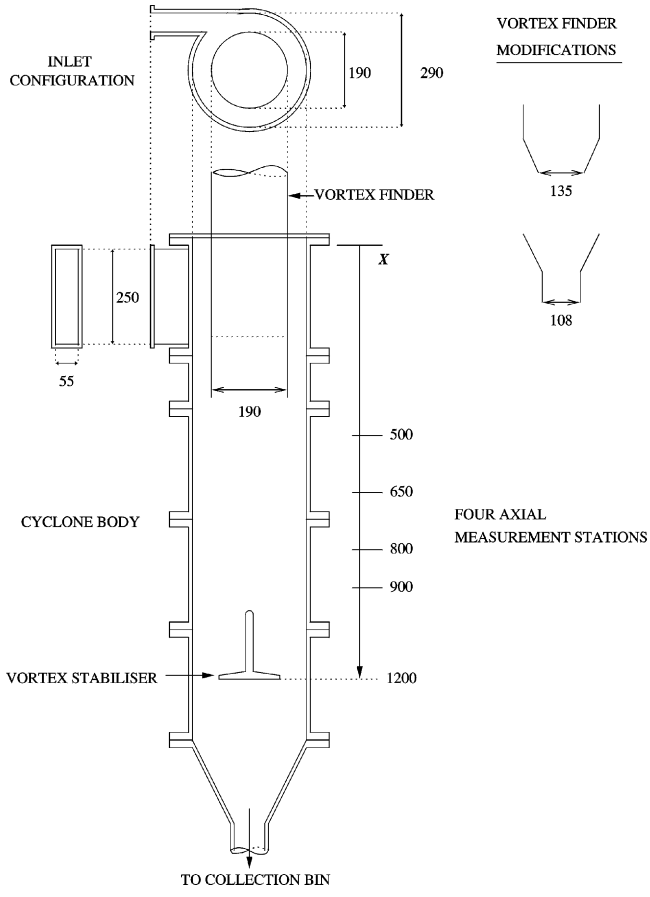

Fig. 1. Schematic representation of studied gas cyclone separator. Dimensions are in millimetre.

2. Experimental facility

2.1. Cyclone geometry

The cyclone investigated (see Fig. 1) consists of a cylindrical body 0.29 m in diameter with a scroll type of inlet to introduce the fluid tangentially. At the base of the cyclone, a sudden reduction of the cross-sectional area occurs owing to the presence of a vortex stabilizer that also serves to reduce re-entrainment of particles from the collection hopper. The air is exhausted through the exit pipe, or vortex finder, at the top of the cyclone. The cyclone is entirely constructed of acrylate elements to facilitate visual observation and to maintain a large geometrical flexibility. Three different cyclone geometries were studied (Fig. 1), where the diameter of the vortex finder was 0.108, 0.135 and 0.190 m, respectively.

The swirling flow in a cyclone is usually characterized by a Reynolds number, Re, as well as by a geometric swirl parameter, S, which is some measure of the ratio of angular to axial momentum. Both parameters can be expressed in terms of geometrical factors and inlet conditions (Gupta et al., 1984)

$$Re = \frac{U_{\text{in}} b}{v}, \tag{1}$$

$$S = \frac{\pi}{4}\frac{d_e D}{ab}. \tag{2}$$

Generally, industrial gas cyclones are operated under high Re-numbers ($\sim 10^5$) and swirl numbers varying between 1.5 and 4.0. For the cases considered here, the swirl numbers amounted to 1.8, 2.2, and 3.1, corresponding to vortex finder diameters of 0.108, 0.135, and 0.190 m, respectively. Experiments were carried out at a moderate Re-number of 2.5×10^4 (inlet velocity of $6.2\ \text{m s}^{-1}$).

2.2. Experimental equipment

Tangential and axial velocity components along the radius of the cyclone were measured by use of two-component laser-Doppler velocimetry. The LDV was operated in backscatter mode, and signal processing was performed with a Doppler burst correlator of TSI (IFA 750). The laser beams were focused by a 250 mm lens to

obtain a measurement volume approx. 0.78 mm in length and 0.078 mm in width. Due to the cyclone wall thickness of 5.0 mm, the two measurement volumes did not coincide completely at all radial positions. Hence, no turbulent cross-correlations (Reynolds shear stress) could be measured.

As a result of the separation characteristics of a cyclone, LDV measurements may be complicated by a low concentration of seeding particles in the vortex core. A seeding system was designed to provide the main flow line with droplets some 2 μm in diameter. A water/glycerol solution was fed into a pressured air atomizer and injected into a knock out vessel (in fact a crude cyclone) to remove large droplets. At the conditions studied, it was still possible to obtain data rates (i.e. number of velocity measurements per unit time) near the centerline of some 50 Hz. Data rates in the outer region of the flow field amounted to 800 Hz. The mean and RMS velocity for each radial position were calculated from $1–3 \times 10^4$ data points per channel.

3. Results of the experiments

3.1. Mean velocity profiles

Velocity profiles were measured along the cyclone radius at four axial stations in the separation zone of the cyclone (see Fig. 1). The measured mean tangential and axial velocity components for the three cyclone geometries studied are presented in Figs. 2 and 3, respectively.

For all vortex finder diameters, the swirl distribution shows the expected Burgers' type of vortex, consisting of an outer free vortex and a solid-body rotation at the core region. The profiles, nevertheless, differ quite strongly in size of the core region, and in maximum tangential velocity. A reduction of the vortex finder diameter results in a sharp increase of the maximum tangential velocity from 1 to 2.5 times the inlet velocity. Further, the free-vortex profile in the outer region is affected by the diameter of the vortex finder.

The tangential velocity profiles at various axial stations are rather similar. Due to wall friction, tangential velocities exhibit a drop close to the wall. For the large vortex finder diameter, the vortex core is widening near the vortex finder due to loss of swirl in the exit pipe. This core widening is less pronounced for the other cases.

The shape of the axial velocity profiles is also affected by the cyclone geometry (see also Fig. 3). The edge of the core region corresponds with the maximum axial velocity, and for most profiles, the vortex core exhibits a dip in the axial velocity or even reverse flow. This may be explained by loss of swirl in the exit pipe, which results in an adverse (positive) pressure gradient at the centerline. Hence, fluid with less swirl is drawn back from the exit pipe into the cyclone. Near the wall, the gas is flowing downwards. As a result of radial inflow the downflow becomes weaker while proceeding towards the vortex

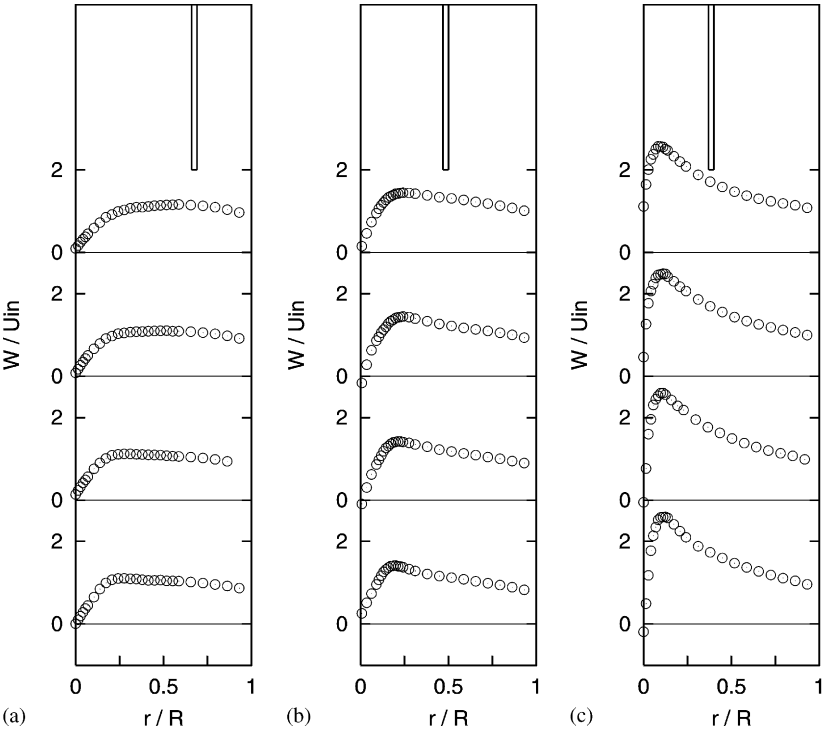

Fig. 2. Radial profiles of the mean tangential velocity at four axial measurement stations in the separation section of a gas cyclone for three geometric swirl numbers: $S = 3.1$ (a), 2.2 (b) and 1.8 (c). All profiles are normalized by the inlet velocity $U_{in} = 6.2\ m\ s^{-1}$.

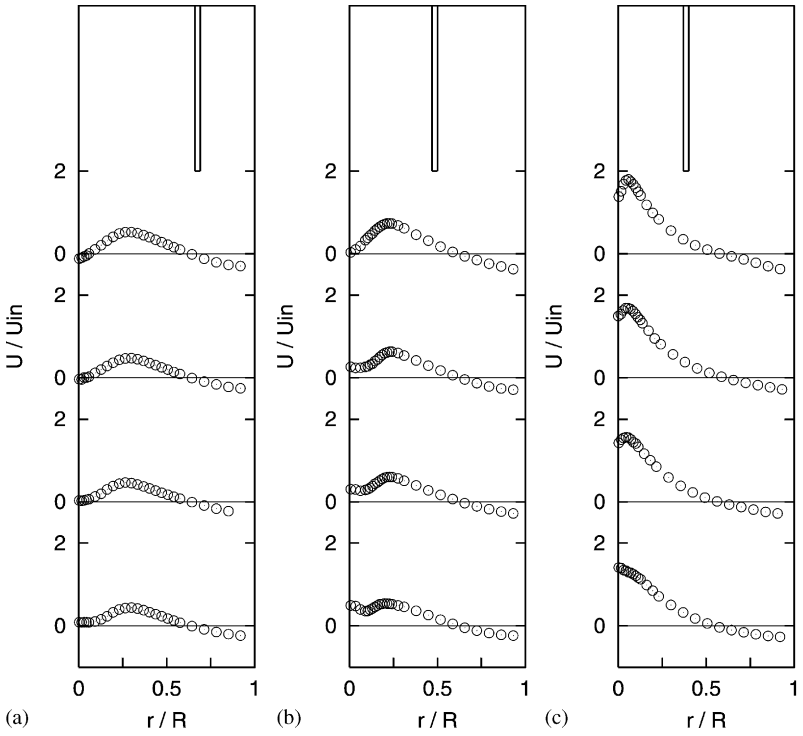

Fig. 3. Radial profiles of the mean axial velocity normalized by the inlet velocity $U_{in} = 6.2\,m\,s^{-1}$. For experimental conditions see caption Fig. 2.

stabilizer. The effect of the vortex finder diameter on the axial flow field is considerable; the maximum axial velocity is increased to some two times the inlet velocity. The vortex stabilizer near the bottom of the gas cyclone appears to inhibit the axial flow reversal near the cyclone axis. Its effect is limited to the flow region in the lower part of the separation zone.

The measured mean velocity profiles show that the centrifugal field as well as the axial flow field strongly depend on the vortex finder diameter. In general, strongly swirling flow in a cyclone is not only determined by the internal geometrical layout, but also becomes sensitive to conditions downstream the cyclone itself. This flow condition is called subcritical, since inertial disturbances are permitted to propagate upstream (Hogg and Leschziner, 1989).

3.2. Turbulence measurements

In Fig. 4, samples of two LDV time series are shown. The two signals originate from the same LDV channel, and relate to the centreline of the cyclone and the wall region, respectively. The time series represent the fluctuating tangential velocity component as a function of time made dimensionless by a macro timescale $T \doteq D/U_{in}$. There is a non-equidistant distribution of data points due to the Poisson statistics governing the particle arrival time in the measurement volume.

The data show the presence of turbulent fluctuations superimposed on a low-frequency oscillation, as may be shown more clearly by spectral analysis of the time series (see Hoekstra et al., 1998b). This oscillation is due to the precessing vortex core (PVC), which is a hydrodynamic instability often observed in strongly swirling flow. The PVC introduces pseudo-turbulence if velocity measurements are performed by means of one-point techniques, such as LDV. The PVC may also account for the small axi-asymmetry with respect to the geometrical centreline that is present at all measurement stations presented in Figs. 2 and 3 (see also Hoekstra et al., 1998a). The dynamic behaviour of cyclonic flow may be characterized by the Strouhal number, $St \doteq f_{prec} D/U_{in}$, which for high Reynolds numbers tends to a constant value (Gupta et al., 1984), in our case 0.6. This implies that the precession frequency is proportional to the inlet velocity.

Especially the core region is affected by the PVC. This is due to the large radial gradients of the tangential as well as the axial velocity components in the vortex core. As shown by the measurement results on the mean flow field (Figs. 2 and 3), the swirl number largely determines the size of the vortex core and the magnitude of the mean velocity gradient. Hence, it is to be expected that the diameter of the vortex finder affects the magnitude of the measured RMS in the core region. This will become more clear in the section on flow predictions, where measured u' and w' profiles are compared to results of calculations.

The PVC also affects the measured mean velocity profiles (Hoekstra et al., 1998b). This implies that considerable caution is needed if LDV data on the gas flow in a cyclone are applied to validate numerical simulations,

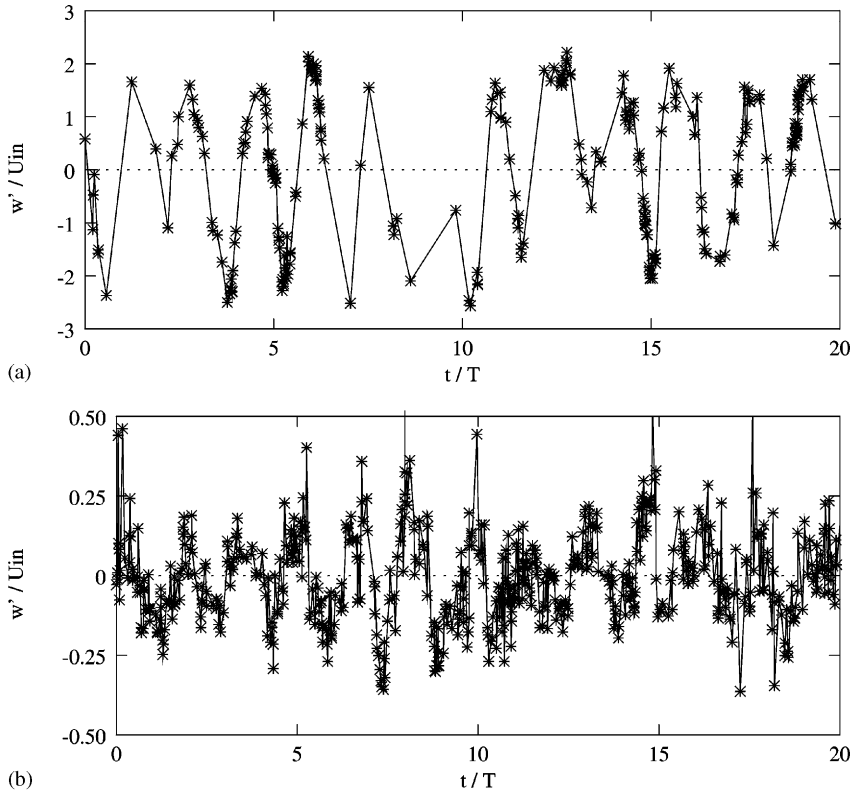

Fig. 4. Two samples of LDV time series made dimensionless by a timescale, $T = 47$ ms, and inlet velocity $U_{in} = 6.2\ \mathrm{m\,s^{-1}}$. Recorded at measurement station $x = 500$ mm, and radial position (a) $r/R = 0.0$ and (b) $r/R = 0.3$.

which are based on the discretization of the Reynolds averaged Navier–Stokes (RANS) equations. This kind of simulations do not take the presence of a low-frequency oscillation, such as the PVC, into account. Especially in comparing RMS measurements and simulations, one has to bear in mind that part of the measured RMS near the centreline is due to the PVC, and should be considered as pseudo-turbulence.

4. Numerical model

4.1. Numerical framework

A conventional way of modelling strongly swirling flow in a gas cyclone is to assume incompressible, steady, and axi-symmetric flow. These assumptions facilitate the mathematical formulation of the problem by simplifying $(\partial/\partial\theta = 0)$ the continuity equation and the averaged Navier–Stokes equations for transport of momentum, which, respectively, may be written as:

$$\frac{\partial U}{\partial x} + \frac{1}{r}\frac{\partial rV}{\partial r} = 0, \tag{3}$$

$$\rho\left(U\frac{\partial U}{\partial x} + V\frac{\partial U}{\partial r}\right) = -\frac{\partial P}{\partial x} + \frac{\partial}{\partial x}t_{xx} + \frac{1}{r}\frac{\partial}{\partial r}r\tau_{xr}, \tag{4}$$

$$\rho\left(U\frac{\partial V}{\partial x} + V\frac{\partial V}{\partial r} - \frac{W^2}{r}\right) = -\frac{\partial P}{\partial r} + \frac{\partial}{\partial x}t_{xr} + \frac{1}{r}\frac{\partial}{\partial r}r\tau_{rr} - \frac{\tau_{\theta\theta}}{r}, \tag{5}$$

$$\rho\left(U\frac{\partial W}{\partial x} + V\frac{\partial W}{\partial r} + \frac{VW}{r}\right) = \frac{\partial}{\partial x}\tau_{x\theta} + \frac{1}{r^2}\frac{\partial}{\partial r}r^2\tau_{r\theta}, \tag{6}$$

where the velocity components (U,V,W) are ensemble averaged through Reynolds decomposition and the stress terms τ_{ij} are the sum of viscous and turbulent (Reynolds) stresses. For the turbulent stresses an additional closure model is needed (see below).

A complication of this computational framework is that the 3D geometry of a gas cyclone has to be converted to an axisymmetric geometry. In the computational model, the gas flow rate is simply imposed by a uniform radial velocity along the height of the inlet section. The inlet configuration of the cyclone studied is of the scroll type, which means that the angular momentum may be defined by the tangential velocity component at the cyclone radius. The turbulence quantities were also uniformly imposed at the inlet by using the following correlations:

$$k_{\mathrm{in}} = \tfrac{3}{2}(IU_{\mathrm{in}})^2, \tag{7}$$

$$\varepsilon_{\mathrm{in}} = C_\mu^{3/4}k_{\mathrm{in}}^{3/2}/l_m, \tag{8}$$

where the turbulence intensity, I, was taken 0.10, C_μ is an empirical constant equal to 0.09, and the characteristic turbulence length scale $l_m = 0.07b$. The computed value of k is used to estimate the Reynolds stresses at the inlet from the assumption of isotropic turbulence, i.e. the normal stresses are set to $2k/3$, and all shear stresses are zero. The predictions appeared to be rather insensitive to the exact initial value for k_{in} and ε_{in}.

The simulations were perfomed by use of the commercial finite volume flow solver Fluent V4.47. The geometrical layout of the cyclone was modelled in a boundary fitted coordinate system, and final solutions were obtained with $\sim$15 000 grid cells. The convective fluxes were approximated by a bounded QUICK-scheme, which is less diffusive than first-order schemes. The boundary conditions at the outlet of the cyclone were prescribed by zero streamwise gradients for all flow variables.

4.2. Turbulence modelling

In the field of modelling confined swirling flow, an important issue is the assessment of the performance of turbulence closure models. The ability of any turbulence model to capture the interaction between swirl and the turbulent stress field is crucial to the predictive performance of the computational scheme (Hogg and Leschziner, 1989). The flow field in a cyclone separator can be considered as a special case of swirling flow, as additional complex flow features, such as axial flow reversal and subcriticality, strongly affect the mean velocity field as well as the turbulence distribution.

Some of the first results on modelling gas cyclone separators by use of CFD were obtained by Boysan et al. (1982). They applied the algebraic stress model (ASM) to compute the six Reynolds stress components. More recent work published on the modelling of cyclonic flow employed the standard k–ε model (Zhou and Soo, 1990), a modified k–ε model (Dyakowski and Williams, 1993), and the RNG-k–ε model (Griffiths and Boysan, 1996), respectively. A more advanced, but computationally more expensive turbulence model, is the full differential Reynolds stress transport model (RSTM), where the transport of each Reynolds stress is described by its own partial differential equation. These equations can be written in a compact form by Cartesian tensor notation as follows:

$$\frac{1}{r}\frac{\partial}{\partial x_k}(\rho r U_k \overline{u_i u_j}) - D_{ij} = P_{ij} - \frac{2}{3}\rho\delta_{ij}\varepsilon + \Phi_{ij} + R_{ij}, \qquad (9)$$

where the term P_{ij} represents the (exact) expression for the generation of the stress $\rho\overline{u_i u_j}$. The terms D_{ij}, Φ_{ij}, and ε are the turbulent diffusion, redistribution of turbulent kinetic energy, and the rate of dissipation, respectively. These three terms need to be modelled. The term R_{ij} arises from the transformation of plane to axi-symmetric coordinates with swirl (see Hogg and Leschziner, 1989).

In Fluent V4.47, they are modelled according to the so-called basic RSTM formulation (also known as the LRRG-model, see e.g. Hanjalić, 1994). The simple-gradient hypothesis is applied for D_{ij}. The dissipation rate, ε, is governed by its own transport equation. This equation basically incorporates the same terms as used by the k–ε-model. In the model for Φ_{ij}, wall-reflection terms are taken into account to selectively damp the fluctuations in the direction normal to the wall. Standard wall functions are used to model the near-wall region of the flow.

5. Predictions

5.1. Mean flow field

The data set on different geometrical layouts of a gas cyclone, as obtained by LDV measurements, may be used to judge the performance of the RSTM in relation to some of the turbulence models mentioned earlier. Fluent V4.47 supports the standard k–ε model, the RNG-k–ε model and the RSTM. The predictions of the three turbulence models on cyclonic flow are presented in Fig. 5, where the mean velocity profiles are compared with experimental results.

For all cases studied, the standard k–ε model predicts a solid-body rotation rather than the expected combined vortex (Fig. 5a, c and e). This was also noticed by Hogg and Leschziner (1989) and Jones and Pascau (1989) for confined strongly swirling flow in a combustion chamber. For rotating flows, where the gradients in the radial direction are dominant, it was demonstrated by Jakirlić (1997) that with an eddy-viscosity closure the W-equation effectively describes a solid-body rotation.

In the RNG-k–ε model, the effect of rotation is included in the calculation of the turbulent viscosity (Griffiths and Boysan, 1996); this results in an improved prediction of the shape of the swirl profile for the large vortex finder case. For the other cases, however, the model still fails to predict the free-vortex distribution in the outer region of the flow.

In contrast to the eddy-viscosity models, the RSTM is capable of reproducing the essential features of the measured W-profiles. The swirl distribution, as predicted by the RSTM, has the pronounced shape of a Burgers' vortex in all cases. A discrepancy, however, is noticed for all vortex finders with respect to the size of the vortex core and the magnitude of the maximum tangential velocity. Similar deviations have been observed for confined vortex flow, which, according to Jones and Pascau (1989), should be attributed to the asymmetry in the measured flow. Part of the deviations, especially with respect to the magnitude of the maximum tangential

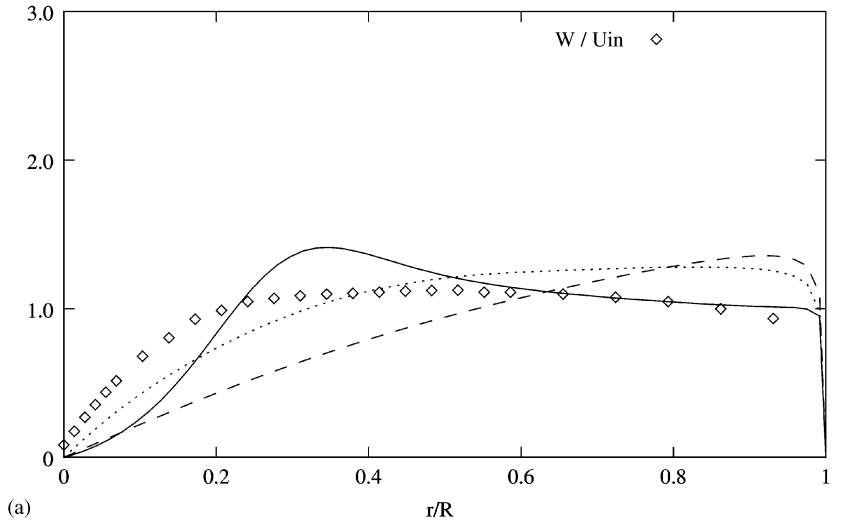

(a)

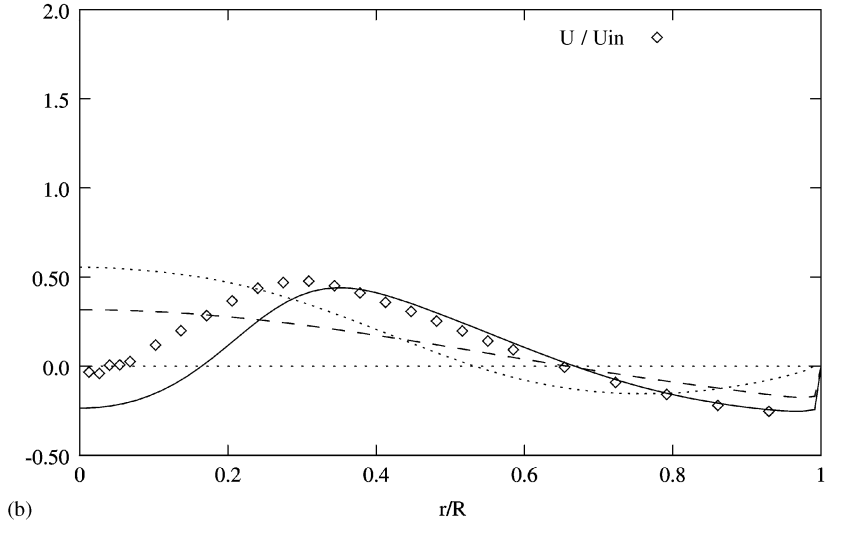

(b)

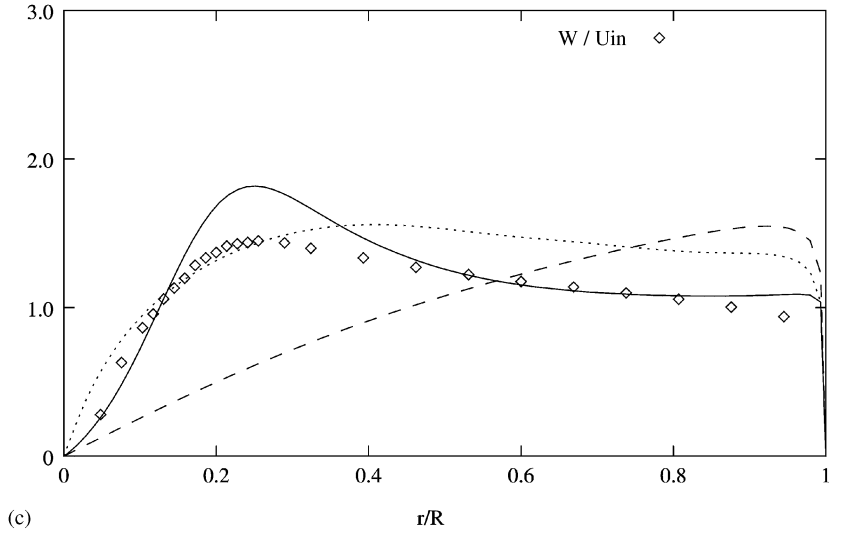

(c)

Fig. 5. Comparison of numerical predictions and measurements of the mean tangential (W) and axial (U) velocity, normalized by the inlet velocity, $U_{in} = 6.2\ m\ s^{-1}$. Results presented for swirl number $S = 3.1$ (a, b), 2.2 (c, d) and 1.8 (e, f) at measurement station $x = 650$ mm: (◇) LDV measurements, (–) RSTM, (· ·) RNG-k–ε, (- -) k–ε.

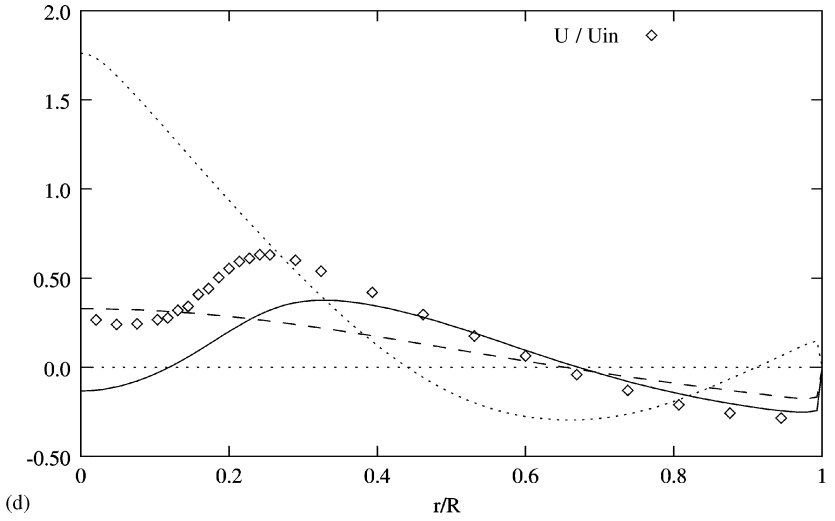

(d)

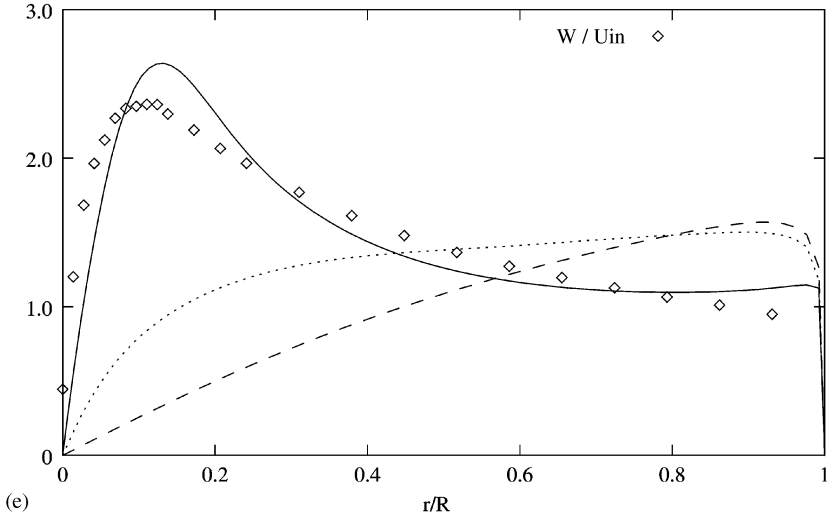

(e)

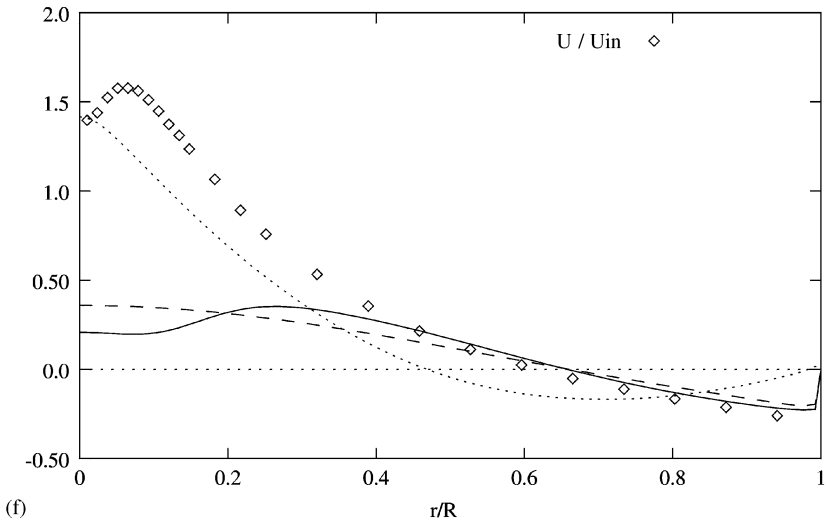

(f)

Fig. 5. Continued.

velocity, may be due to the spatially averaging effect of vortex core precession (Hoekstra et al., 1998b).

Although the use of wall-reflection terms in the pressure–strain correlation is generally considered a necessity (Hanjalić, 1994), a considerable difference between the predicted and measured tangential velocity profiles near the wall still exists. This suggests that, in the current formulation, the wall-reflection terms, originally

introduced for wall-parallel flows, are not suitable for strongly rotating flows.

Only the RSTM is capable of predicting low axial velocities in the vortex core, although for the smallest vortex finder diameter (see Fig. 5f), this is not confirmed by experimental results. For $S = 2.2$ (see Fig. 5e), the RNG-k–ε model predicts an unrealistic upward flow near the cyclone wall. This is related to the shape of the vortex finder, and the existence of a recirculation zone. According to the RNG-k–ε model, this recirculation zone is present near the cyclone wall, whereas the RSTM predicts it close to the vortex finder.

5.2. Fluctuating velocity profiles

Radial profiles of the axial and tangential RMS velocity for the three cyclone geometries are shown in Fig. 6.

Because of the poor performance of the k–ε and RNG-k–ε models in predicting the mean flow field of the gas cyclones studied, only RSTM predictions are plotted. Although results are presented for one axial station only, they are representative of other measurement stations as well. In all cases, the experimental results in the free-vortex region of the flow show an anisotropic distribution of axial and tangential normal stresses. Also, the geometric swirl number does not seem to affect the RMS levels in this region.

The RSTM does predict the anisotropy observed experimentally, but the levels of the two RMS velocities are overpredicted for most cases. Jones and Pascau (1989) suggest that the ε-equation may be the cause of this discrepancy, and that the predicted dissipation levels may be too low. They modified the ε-equation by introducing an additional term that depends on the rotation rate; its effect, however, was a further increase in RMS levels.

Both the RSTM and the k–ε model predictions largely deviate from the experimental results in the vortex core region of the flow. When discussing vortex core precession and its effect on the LDV measurements, deviations between steady-state RANS predictions and experimental results were anticipated. The radial profiles of the axial and tangential RMS velocity presented in Fig. 6 show that the RMS velocities increases near the centreline as a result of the precessing vortex core. The

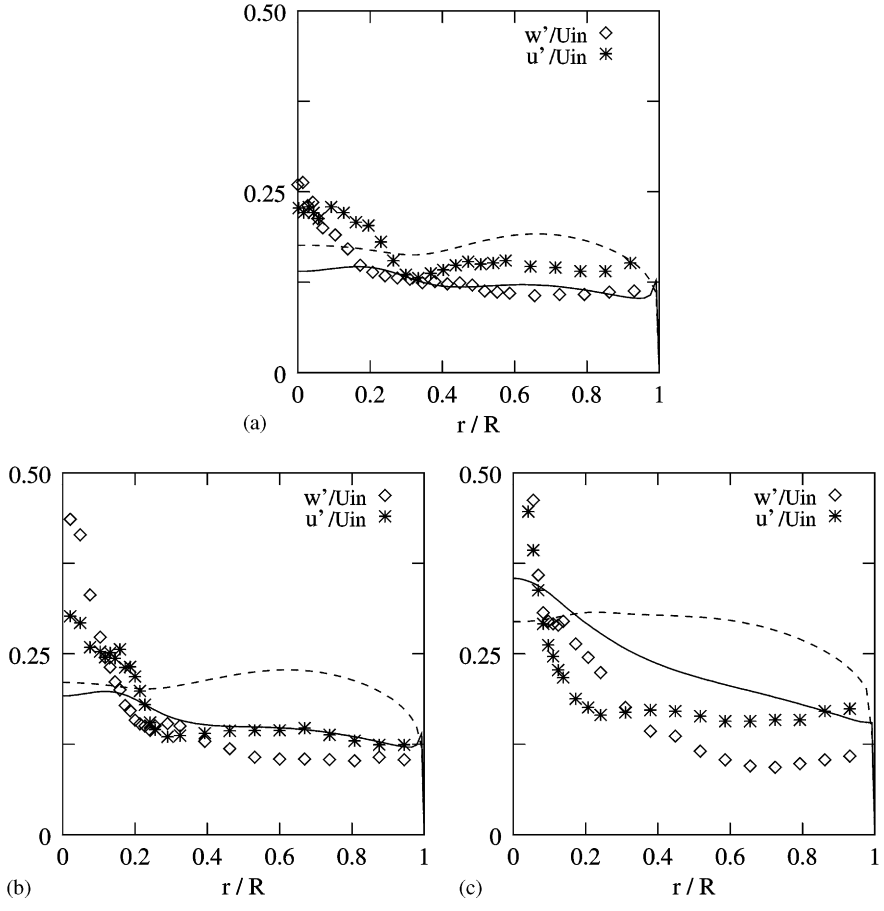

Fig. 6. Comparison of numerical predictions and measurements of the fluctuating tangential (w') and axial (u') velocity, normalized by the inlet velocity, $U_{in} = 6.2\ m\ s^{-1}$. Results presented for swirl number $S = 3.1$ (a), 2.2 (b) and 1.8 (c) at measurement station $x = 650$ mm: Experimental: ($\diamond$) w', ($*$) u'. RSTM prediction: (–) w' , (- -) u'.

magnitude of the RMS velocities in the core region is related to the mean velocity gradients, and hence, the diameter of the vortex finder. The RSTM results show that the axial and tangential RMS levels in the core region are almost constant and equal to each other. This may be confirmed by experiment only if the pseudo-turbulent part of the measured RMS velocities due to vortex core precession can be clearly distinguished.

6. Conclusions

LDV measurements of the axial and tangential velocity in a gas cyclone showed that the gas flow field is strongly affected by the geometric swirl number or exit pipe diameter. Decreasing the exit pipe diameter results in a reduction of the vortex core size and a considerable increase of the maximum tangential velocity. The core region is dominated by the so-called precessing vortex core, which introduces pseudo-turbulent fluctuations in the LDV measurement.

The performance of three turbulence models in predicting the strongly swirling flow in a cyclone was evaluated by comparison with the velocity measurements. Both the k–ε model and the RNG-k–ε model predicted an unrealistic distribution of axial and tangential velocities, and, hence, are unsuitable for cyclonic flow. Results obtained with the Reynolds stress transport model are in reasonable agreement with the experimental data, although still some discrepancies exist which plead for further improvement.

Future extensions of this work include the numerical prediction of the cyclone collection performance. For a specific geometrical layout of a cyclone, this may be done by (1) solving the gas flow field using the Reynolds stress transport model, and (2) Lagrangian tracking of a number of particle size classes to obtain complete grade-efficiency curves. In this way, the performance of a specific cyclone design can be determined in terms of pressure drop and particle cut-size.

Acknowledgements

The authors gratefully acknowledge the support by the Netherlands Foundation for Chemical Research (SON) and the financial aid from the Netherlands Organisation for Scientific Research (NWO) and from Van Tongeren Kennemer BV, Beverwijk, The Netherlands.

Notation

a	cyclone inlet height, m
b	cyclone inlet width, m
d_e	diameter exit pipe, m
D	diameter cyclone body, m
f_{prec}	precession frequency, s^{-1}
h^*	cyclone core height, m
k	turbulent kinetic energy, $\mathrm{m}^2\,\mathrm{s}^{-2}$
r, x	radial and axial position, m
R	cyclone radius, m
Re	Reynolds number, dimensionless
S	swirl number, dimensionless
St	Strouhal number, dimensionless
T	macro timescale, s
u', w'	fluctuating axial and tangential velocity, $\mathrm{m}\,\mathrm{s}^{-1}$
U, W	mean axial and tangential velocity, $\mathrm{m}\,\mathrm{s}^{-1}$
U_{in}	inlet velocity, $\mathrm{m}\,\mathrm{s}^{-1}$
U_k	mean velocity component in the direction x_k, $\mathrm{m}\,\mathrm{s}^{-1}$
v_t	tangential velocity at core radius, $\mathrm{m}\,\mathrm{s}^{-1}$

Greek letters

δ_{ij}	Kronecker delta, dimensionless
ε	dissipation of turbulent kinetic energy, $\mathrm{m}^2\,\mathrm{s}^{-3}$
ν	kinematic viscosity, $\mathrm{m}^2\,\mathrm{s}^{-1}$
ρ	density, $\mathrm{kg}\,\mathrm{m}^{-3}$
τ_{ij}	stress tensor, $\mathrm{kg}\,\mathrm{m}^{-1}\,\mathrm{s}^{-2}$

Abbreviations

CFD	computational fluid dynamics
LDV	laser-Doppler velocimetry
PVC	precessing vortex core
RANS	Reynolds averaged Navier–Stokes equations
RMS	root mean square
RNG	re-normalization group theory
RSTM	Reynolds stress transport model

References

Barth, W. (1956). Berechnung und Auslegung von Zyklonabscheidern auf Grund neuerer Untersuchungen. *Brennst. Wärme Kraft*, *8*, 1–9.

Boysan, F., Ayers, W.H., & Swithenbank, J. (1982). A fundamental mathematical modelling approach to cyclone design. *Trans. Inst. Chem. Engrs*, *60*, 222–230.

Dietz, P.W. (1981). Collection efficiency of cyclone separators. *A.I.Ch.E. J.*, *27*(6), 888–892.

Dyakowski, T., & Williams, R.A. (1993). Modelling turbulent flow within a small-diameter hydrocyclone. *Chem. Engng Sci.*, *48*(6), 1143–1152.

Griffiths, W.D., & Boysan, F. (1996). CFD and empirical modelling of the performance of a number of cyclone samplers. *J. Aerosol Sci.*, *98*, 281–304.

Gupta, A.K., Lilley, D.G., & Syred, N. (1984). *Swir. flows*. Tunbridge Wills, UK: Abacus Press.

Hanjalić, K. (1994). Advanced turbulence closure models: A view of current status and future prospects. *Int. J. Heat Fluid Flow*, *15*(3), 178–203.

Hoekstra, A.J., Israël, A.T., Derksen, J.J., & Van den Akker, H.E.A. (1998a). The application of laser diagnostics to cyclonic flow with vortex precession. *Proceedings of the 9th International Symposium on Applications of Laser techniques to Fluid Mechanics*, Lisbon, Portugal (Vol. 1, p. 4.3).

Hoekstra, A.J., Van Vliet, E., Derksen, J.J., & Van den Akker, H.E.A. (1998b). Vortex core precession in a gas cyclone. *Advances in turbulence VII* (pp. 289–293). Dordrecht: Kluwer Academic Publishers.

Hogg, S., & Leschziner, M.A. (1989). Computation of highly swirling confined flow with a Reynolds stress turbulence model. *AIAA J.*, *27*, 57–63.

Iozia, D.L., & Leith, D. (1989). Effect of cyclone dimensions on gas flow pattern and collection efficiency. *Aerosol Sci. Technol.*, *10*, 491–500.

Jakirlić, S. (1997). *Reynolds-Spannungs-Modellierung Komplexer Turbulenter Strömungen*. Ph.D. thesis, Universität Erlangen-Nürnberg, Herbert Urtz Verlag, München.

Jones, W.P., & Pascau, A. (1989). Calculation of confined swirling flows with a second moment closure. *ASME J. Fluids Engng.*, 111, 248–255.

Leith, D., & Licht, W. (1972). The collection efficiency of cyclone type particle collectors – a new theoretical approach. *A.I.Ch.E. Symp. Series*, *68*(126), 196–206.

Stairmand, C.J. (1951). The design and performance of cyclone separators. *Trans. Inst. Chem. Engrs*, *29*, 356–383.

Zhou, L.X., & Soo, S.L. (1990). Gas–solids flow and collection of solids in a cyclone separator. *Powder Technol.*, *63*, 45–53.